Journal of Non-Newtonian Fluid Mechanics 189-190 (2012) 8–13

Phase-field simulations of dynamic wetting of viscoelastic fluids

Pengtao Yue[a,*], James J. Feng[b,c]

[a] *Department of Mathematics, Virginia Tech, Blacksburg, VA 24061-0123, USA*
[b] *Department of Chemical and Biological Engineering, University of British Columbia, Vancouver, BC V6T 1Z3, Canada*
[c] *Department of Mathematics, University of British Columbia, Vancouver, BC V6T 1Z2, Canada*

Abstract

We use a phase-field model to simulate displacement flow between a Newtonian and a viscoelastic fluid in a two-dimensional channel. The viscoelastic fluid is described by the Oldroyd-B model and the stress singularity at the contact line is regularized by the Cahn-Hilliard diffusion. In a small region near the contact line, the flow field features a large shear rate that produces a high polymer stress even at relatively low wetting speed. This polymer stress pulls the interface toward the viscoelastic fluid. As a result, the viscous bending at the contact line is enhanced when the advancing fluid is viscoelastic and weakened when the receding fluid is viscoelastic. However, the overall effect is limited by the small size of this strong shear region. These results are consistent with experimental observations. By examining the flow and stress field in the neighborhood of the contact line, we find that viscoelastic stress growth within a finite residence time provides a plausible explanation of the curious experimental observation that the contact line is affected by the viscoelasticity of the oligomeric solvent rather than the high molecular-weight polymer solute.

Keywords: contact angle, Oldroyd-B, diffuse-interface method, first normal stress difference

*Corresponding author
Email addresses: ptyue@math.vt.edu (Pengtao Yue), jfeng@chbe.ubc.ca (James J. Feng)

1. Introduction

The contact-line dynamics plays an important role in many industrial applications such as coating, printing, and enhanced oil recovery. At moving contact lines, the conventional Navier-Stokes formulation runs into a non-integrable stress singularity [1, 2]. Different models have been proposed to relieve the stress singularity, e.g., by using a precursor film [3], slip [4], and diffusion [5]. For Newtonian fluids, the qualitative behavior of the wedge-like flow in the outer region does not depend on the detailed physics in the inner region where the singularity is relaxed [4, 6]. It is therefore not surprising that different models generate consistent results at the macroscopic length scale when film thickness, slip length, and diffusion length are appropriately matched [3, 7].

The liquids in the aforementioned applications are often non-Newtonian, and their rheology is known to affect the *outer flow* at the contact line. For example, Min *et al.* [8] compared the dynamic wetting in different flow geometries in the sessile drop method and the Wilhelmy plate method for measuring surface tension. They reported that the wetting dynamics, i.e., the relationship between the apparent contact angle and the contact line speed, is independent of flow geometry in Newtonian fluids, while it is dependent on flow geometry in non-Newtonian fluids, including polymer solutions and a suspension of silica nanoparticles. The explanation lies in the fact that the macroscopic flow geometry influences the shear rate and effective viscosity in the bulk flow, and therefore affects the whole wetting dynamics in the non-Newtonian fluids.

Perhaps more interestingly, the structure and rheology of complex fluids may also affect the *inner region* of contact line. Ramé *et al.* [9] found that the length scale and microscopic contact angle that characterize the inner physics have a detectable dependence on the spreading velocity when a polydimethylsiloxane (PDMS) liquid displaces air. They explained this dependence by the additional time scale brought into the inner region by the PDMS polymer. As the silicone oils used have very short relaxation times, one may expect even larger effects for polymeric liquids having stronger elasticity.

Of the numerous studies on non-Newtonian effects in coating flows, most have focused on the coated film [10, 11, 12, e.g.] and only a few have dealt directly with the moving contact line. Frayssee and Homsy [13] studied the fingering instability of a Boger fluid in spin coating. In their experiment, the Weissenberg number was small and the Boger fluid behaved essentially as its

Newtonian solvent. Garoff and co-workers conducted a series of experiments on dynamic wetting by immersing a cylinder into a bath of polymer liquid at a constant speed [14, 15, 16, 6, 17]. By comparing the steady interface shape with that from the asymptotic analysis in Newtonian fluids [18], they observed that the non-Newtonian effect was confined to the close vicinity of the contact line. In this inner region, the viscous bending of interface is reduced by shear thinning and enhanced by viscoelasticity [15, 16].

A surprising discovery of these experiments is the following. The Boger fluids used consist of high molecular-weight (HMW) polystyrene (PS) or polyisobutylene (PIB) dissolved in their respective oligomeric base fluids [19]. When the Boger fluids are replaced by their oligomeric solvents, the same amount of extra bending of the interface is obtained. Apparently, the effect does not arise from the HMW polymer solute but from the lower molecular-weight solvent. This contravenes the conventional wisdom that viscoelastic effects are expected to first arise from the longest polymer relaxation times. Up to now this has remained a mystery.

The numerical simulation of dynamic wetting in viscoelastic fluids is complicated by the fact that unlike its Newtonian counterpart, the macroscopic flow is now sensitive to the detailed physics in the inner region. For example, Spaid and Homsy [20] simulated spin coating and reported that the viscoelastic effect on the capillary ridge differed for the precursor film model and the slip model. So it is natural to expect different results from different contact-line models. In this paper, we will study how viscoelasticity affects the contact line dynamics in the phase-field model, and whether this model correctly predicts experimental observations. Our results suggest an explanation for the aforementioned mystery.

2. Formulations

We consider the displacement between an immiscible pair of fluids, one Newtonian and the other viscoelastic (Oldroyd-B), in a two-dimensional channel between two parallel plates (Fig. 1). We introduce a phase-field variable ϕ to describe the diffuse interface, $\phi = 1$ in the viscoelastic fluid and $\phi = -1$ in the Newtonian fluid. The governing equations consist of the Cahn-Hilliard equation for the interface, the momentum equation, the incompressible continuity equation, and the constitutive equation for the viscoelastic fluid:

$$\frac{\partial \phi}{\partial t} + \boldsymbol{v} \cdot \phi = \gamma \nabla^2 G, \tag{1}$$

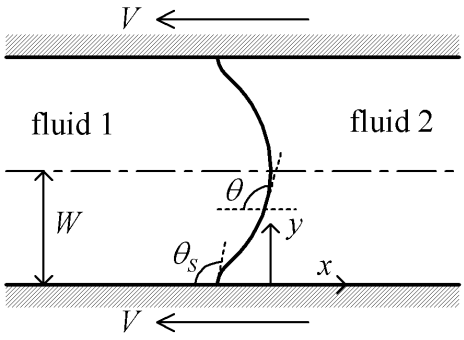

Figure 1: Steady displacement flow of two immiscible fluids between parallel plates, viewed in a reference frame attached to the steadily moving contact line. θ_S is the static contact angle, and θ gives the slope of the interface.

$$\rho\left(\frac{\partial \boldsymbol{v}}{\partial t}+\boldsymbol{v}\cdot\nabla\boldsymbol{v}\right)=\nabla(-p\boldsymbol{I}+\boldsymbol{\tau})+G\nabla\phi, \tag{2}$$

$$\nabla\cdot\boldsymbol{v}=0, \tag{3}$$

$$\boldsymbol{\tau}_p+\lambda_H\tau_{p(1)}=\mu_p\left[\nabla\boldsymbol{v}+(\nabla v)^T\right], \tag{4}$$

where

$$G=\lambda\left[-\nabla^2\phi+\frac{\phi(\phi^2-1)}{\epsilon^2}\right] \tag{5}$$

is the chemical potential and

$$\boldsymbol{\tau}=\left(\frac{1+\phi}{2}\mu_s+\frac{1-\phi}{2}\mu_n\right)\left[\nabla\boldsymbol{v}+(\nabla v)^T\right]+\frac{1+\phi}{2}\boldsymbol{\tau}_p \tag{6}$$

is the total stress. Here γ is the Cahn-Hilliard mobility parameter, ϵ is the capillary width which is proportional to the interfacial thickness, λ is the mixing energy density which is related to interfacial tension σ by $\sigma=\frac{2\sqrt{2}}{3}\frac{\lambda}{\epsilon}$ [21]. $\boldsymbol{\tau}_p$ is the polymer stress, λ_H is the polymer relaxation time, μ_s and μ_p are the solvent and polymer viscosities of the Oldroyd-B fluid, μ_n is the viscosity of the Newtonian fluid. The subscript $_{(1)}$ denotes the upper convected derivative [22]. Yue *et al.* [7] showed that the mobility parameter γ together with an effective viscosity μ defines a diffusion length $l_D=\sqrt{\gamma\mu}$ that plays a similar role to the slip length in the slip models. A more detailed discussion of the phase-field theory for contact lines can be found in [7, 23, 24].

The following boundary conditions are imposed on the solid substrate:

$$\boldsymbol{v} = -V\boldsymbol{e}_x, \tag{7}$$

$$\boldsymbol{n} \cdot \nabla G = 0, \tag{8}$$

$$\lambda \boldsymbol{n} \cdot \nabla \phi + f_w'(\phi) = 0, \tag{9}$$

where V is the wall speed, $\boldsymbol{n}$ is the outward pointing normal to the boundary, and f_w is the wall energy that is related to the static contact angle θ_S by [7]

$$f_w(\phi) = -\sigma \cos\theta_S \frac{\phi(3-\phi^2)}{4}. \tag{10}$$

Equation (7) is the no-slip condition and the Eq. (8) enforces zero mass flux across the solid boundary. The contact angle is imposed through Eq. (9). Here we neglect the wall energy relaxation [23] and assume that the microscopic contact angle is fixed at θ_S. Parabolic velocity profiles are imposed at the ends of the channel in a way such that the walls are in motion and the interface is stationary.

In this work we neglect inertia as it does not contribute to the discussions on viscoelasticity. The problem is governed by the following dimensionless groups:

$$Ca = \frac{\mu V}{\sigma} \quad \text{(capillary number)}, \tag{11}$$

$$Cn = \frac{\epsilon}{W} \quad \text{(Cahn number)}, \tag{12}$$

$$S = \frac{l_D}{W} = \frac{\sqrt{\gamma\mu}}{W}, \tag{13}$$

$$\theta_S \quad \text{(static contact angle)}, \tag{14}$$

$$\eta = \frac{\mu_n}{\mu_s + \mu_p} \quad \text{(viscosity ratio)}, \tag{15}$$

$$\beta = \frac{\mu_s}{\mu_s + \mu_p} \quad \text{(retardation-relaxation time ratio)}, \tag{16}$$

$$Wi = \frac{\lambda_H V}{W} \quad \text{(Weissenberg number)}, \tag{17}$$

where μ is a properly defined effective viscosity, W is the macroscopic length scale, which we take to be the half channel width. Here S is the dimensionless diffusion length, a diffuse-interface counterpart of the slip length.

Initially the interface is vertical at the middle of the domain, and we abruptly impose the prescribed parabolic velocity profiles at the ends of the channel as well as the corresponding wall velocity V. The interface deforms in time until a steady state is achieved. The governing equations are solved by a finite-element method on an adaptive triangular mesh that adequately resolves the interfacial region. The streamline upwind Petrov-Galerkin method is used for the constitutive equation (4) to improve stability. All the time-dependent equations are integrated using a second-order accurate, fully implicit time-marching scheme. Details of the numerical algorithm and validation can be found in [25].

3. Results and discussions

We consider a channel of dimensions $6W \times 2W$, which is long enough so that the fully developed velocity profiles at the ends are not affected by the interface at the center of the channel. Due to symmetry, only the lower half of the domain is calculated. The following parameters are chosen unless otherwise specified: $\theta_S = 90°$, $\beta = 0.5$, $\eta = 1$, $Cn = 0.005$, $S = 0.01$. Note that we have matched the total viscosity of the two fluids: $\mu_n = \mu_s + \mu_p = \mu$, which is used as the effective viscosity in defining Ca and S. Besides, the interfacial thickness is small enough to satisfy the criterion $Cn < 4S$, such that the sharp interface limit is achieved [7].

The effect of viscoelasticity on the displacement flow is manifested by the shape of the interface. Figure 2(a) shows that when the advancing fluid is Oldroyd-B (the O/N curves), increasing Wi causes the interface to bend more into the displacing fluid. This trend is reversed when the receding fluid is Oldroyd-B (the N/O curves). The interface slope θ as a function of y is plotted in Fig. 2(b) to further illustrate the bending of the interface. Judging from the slope of the curves near $y = 0$, the O/N interface has the highest curvature while the N/O interface has the lowest curvature near the contact line. In other words, the viscoelasticity in the advancing fluid enhances viscous bending while the viscoelasticity in the receding fluid reduces viscous bending. The former is consistent with the experimental observations by Wei *et al.* [16], where the advancing fluid is viscoelastic. Figure 3 shows the variation of the interface shape when the viscoelastic parameters Wi and β are changed. Overall, the interface only deviates mildly from the Newtonian case, which is again consistent with the experimental observations. In the following, we will explore the detailed flow field and analyze how viscoelasticity

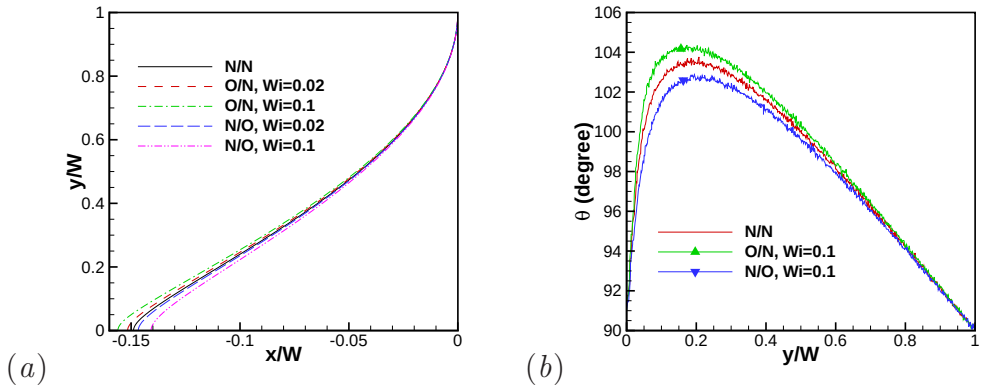

(a) (b)

Figure 2: Interface (a) shapes and (b) slopes at $Ca = 0.02$. O/N refers to the Oldroyd-B fluid displacing the Newtonian fluid and O/N means the inverse. The displacing fluid is to the left of the interface in (a). θ is the angle subtended by the tangent line to the interface and the solid substrate, as illustrated in Fig. 1.

affects the bending of the interface.

The flow field, as illustrated in Fig. 4(a), has a stagnation point at B. The incoming streamlines AB and CB collide and then depart hyperbolically, creating a planar extensional flow at B. Note that the streamlines closely resemble those of an advancing meniscus over a precoated thin film [26], if we view BC as the thin film and AB as the free surface moving rightward. At B, the polymers experience strong stretching and develop large stress gradients, limiting the computable Wi to $Wi \leq 0.1$. But the extensional stress is spatially localized and has little effect on the interface. The region below B and next to the solid wall is characterized by strong shearing. This flow field is essentially the same as that in the Newtonian system. As Yue *et al.* [7] demonstrated, the thickness of this region is roughly $D \approx 2.5 l_D$, l_D being the diffusion length. Thus the local shear rate is $V/D \approx \frac{1}{2.5S}(V/W) = 40(V/W)$ in this calculation with $S = 0.01$. This estimation is borne out by the numerical data of Fig. 4(b), where we have drawn a box around the region of strong shear. The strong shear produces a large first normal stress difference in the polymer, and the polymer stress τ_{pxx} reaches a high level as shown in Fig. 4(c). This extra stress pulls the interface toward the viscoelastic fluid (Fig. 4(d)), which has to be balanced by the Laplace pressure generated by additional bending of the interface. If the Oldroyd-B fluid is receding, τ_{pxx}

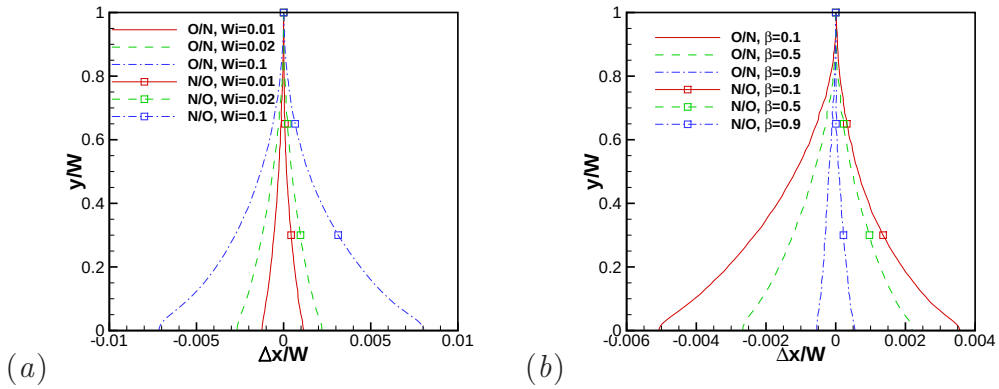

Figure 3: Variation of the interfacial shape at the contact line with the viscoelastic parameters. Δx is calculated by subtracting the x coordinate of the interface in N/N, and $Ca = 0.02$. (a) Wi varies while $\beta = 0.5$ is fixed. (b) β varies while $Wi = 0.02$ is fixed.

will appear on the right side of the interface, and will pull toward the right against the viscous stress and therefore reduce viscous bending. Thus, τ_{pxx} is the cause of the effects observed in Fig. 2. However, because of the small size of this high shear region, the overall effect on the interface is mild.

The numerical predictions above agree qualitatively with the experimental observations of Wei *et al.* [16, 6, 17]. To connect the simulations to reality, we note two points about the model parameters. First, Yue *et al.* [7] showed that the length D corresponds to the slip length l_s in sharp-interface models. By equating the two, the phase-field model generates the same result as the Cox theory [27]. Second, the slip length l_s in *real flows* tends to be much smaller than the numerical value of l_D used in our calculations. Take the immersing tube experiments for example [9]. The macroscopic length scale is the capillary length, on the order of 1 mm. The slip length l_s ranges from 1 to 10^2 nm. Thus the ratio $\delta = l_s/W$ falls between 10^{-6} and 10^{-4}, 2 to 4 orders of magnitude smaller than the numerical S value. This means that in the experiment, the local shear rate near the contact line may get quite high. As to be seen below, this will be a key factor in explaining the anti-intuitive experimental observation of viscoelastic effects due to the solvent.

In the following, we interrogate the flow and transient stress growth in the neighborhood of the contact line in order to rationalize the observation that the viscoelastic effect on the contact line comes not from the HMW

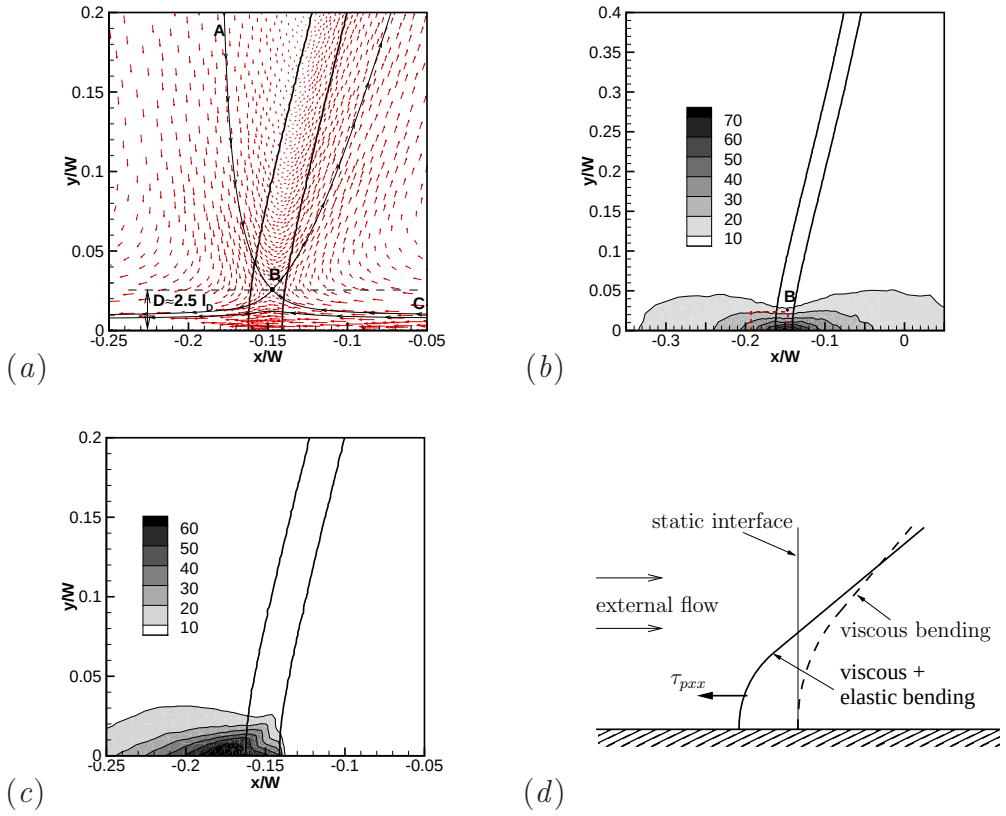

Figure 4: Flow field at the contact line when an Oldroyd-B fluid (left) displaces a Newtonian fluid (right). $Ca = 0.02$, $Wi = 0.02$. (a) The velocity field illustrated by vectors. The two more or less vertical curves, for $\phi = \pm 0.9$, roughly mark the boundaries of the diffuse interface, and the other three solid curves indicate streamlines in the extensional and shearing region of the flow. (b) Contours of the dimensionless shear rate $\frac{\partial u}{\partial y}/(\frac{V}{W})$. The dashed box indicates the high shear region in which the shear rate is above half of the maximum value in most of the area. (c) Contours of the xx component of the dimensionless polymer stress: $\tau_{pxx}/(\mu\frac{V}{W})$. (d) A cartoon showing the extra bending of interface due to polymer stress.

polymer solute but the oligomeric solvent [19, 28]. For this purpose, we first note that upon inception of a simple shear flow $(u, v) = (0, y\dot{\gamma})$, the normal stress τ_{pxx} grows in time as [22]

$$\tau_{pxx} = \left[\lambda_H\dot{\gamma} - \dot{\gamma}(t + \lambda_H)e^{-t/\lambda_H}\right] 2\mu_p\dot{\gamma}. \tag{18}$$

In Fig. 4(b), the strong shear is limited to a narrow region centered at the contact line, and a polymer molecule has a *finite residence time* inside this region: $t_r \approx \frac{\alpha D}{V}$, where α is the aspect ratio of the high-shear region in Fig. 4(b). If we define a local Weissenberg number $Wi^* = \lambda_H \dot{\gamma} \approx \lambda_H \frac{V}{D}$, it can be shown that the polymer stress achieved within the residence time t_r is

$$\tau_{pxx} = \left[Wi^* - (\alpha + Wi^*)e^{-\alpha/Wi^*}\right] 2\mu_p \dot{\gamma}. \tag{19}$$

If we fix $\dot{\gamma}$ and vary the polymer relaxation time λ_H, τ_{pxx} achieves a maximum at an intermediate $Wi^* = Wi_c^* = 0.5576\alpha$. Polymer stress τ_{pxx} is proportional to Wi^* when $Wi^* \ll Wi_c^*$ and proportional to $1/Wi^*$ when $Wi^* \gg Wi_c^*$. Therefore, the high shear region of Fig. 4 only favors a certain range of polymer relaxation times. If we take $\alpha \approx 2$ according to the shear rate contours to the left of the interface (c.f. the dashed box in Fig. 4b), the maximum viscoelastic effect is attained at $Wi_c^* \approx 1$. Note that this Wi_c^* is an order-of-magnitude estimation since the flow field near the contact line is not exactly simple shear. In the simulations (Figs. 2 and 3a), for example, the viscoelastic effect increases with Wi up to $Wi = 0.1$, which corresponds to $Wi^* = 4$. Possibly it peaks at a higher Wi, which is beyond the capability of our numerical tool.

For typical experimental parameters $V = 5 \times 10^{-6}$ m/s and $D = 10^{-8}$ m, this Wi_c^* corresponds to a critical relaxation time $\lambda_{Hc} \approx 0.002$ s, which is of the same order as the relaxation times of the oligomeric PIB and PS solvents. On the other hand, the relaxation time of the HMW polymers in the Boger fluids ranges roughly from 0.02 s to 3 s, much larger than λ_{Hc}. Therefore, in the low speed experiments by Garoff and co-workers, the strong shear in the inner region only excites the elastic modes in the solvent while still keeping the HMW polymers coiled. This explains why the contact line is affected by the non-Newtonian rheology of the oligomeric solvent, not the HMW polymeric solute.

We should point out that most experiments are done with Boger fluids in air, and the contact angles are very close to 0°. The phase-field model imposes the contact angle through the normal gradient of ϕ, whose value is also affected by the ϕ profile across the diffuse interface if $\theta_S \neq 90°$. If θ_S is very close to 0° or 180°, the interface is nearly parallel to the wall and the normal gradient of ϕ is subject to large numerical errors. The results become unreliable in such cases. In general, we can handle the contact angles $\theta_S \in [15°, 165°]$ with confidence. Another source of numerical error is the

vanishingly small air-liquid viscosity ratio. These errors may contaminate the already minute viscoelastic effects and make the analysis unreliable. Figure 5 shows a simulation using parameters closer to the experimental ones. We can see that the viscoelastic curves almost coincide with the Newtonian one, and it is difficult to tell whether this is physical or due to numerical errors associated with the small η and the relatively small θ_S. Fortunately, these deficiencies do not affect the qualitative conclusions made with $\theta_S = 90°$ and $\eta = 1$.

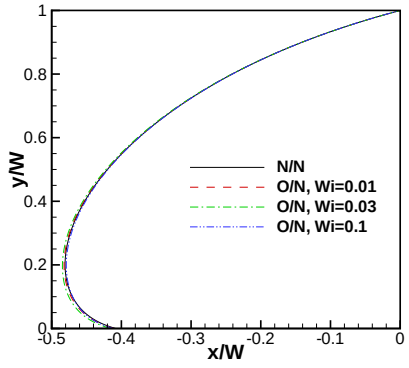

Figure 5: Interface shapes at a small contact angle and a small viscosity ratio. $\theta_S = 30°$, $\beta = 0.5$, $\eta = 0.02$, $S = l_D/W = 0.01$, $Ca = \frac{(\mu_s+\mu_p)V}{W} = 0.1$. Note that l_D is defined as $l_D = \sqrt{\gamma\mu} = \sqrt{\gamma\sqrt{\mu_n(\mu_s+\mu_p)}}$ for unmatched viscosities [7].

Finally, we note that Cahn-Hilliard diffusion is a phenomenological mechanism used to explain the transport of fluids near the contact line. As such, it does not necessarily reflect molecular-scale physics in reality. For example, in the inner region, the fluid particles go across the diffuse interface by convection and then come back by diffusion. In simulating liquid-vapor flows, this constitutes a reasonable representation of evaporation and condensation [29, 30]. For the polymer solution in the present study, however, such mass transport does not have a physical basis. Then where do the polymers go in reality after crossing the interface? One possible scenario is for the polymers to be simply left on the solid substrate, similar to what happens to DNA molecules during molecular combing, spin-stretching, and air-blowing [31, 32].

4. Summary

In this paper, we studied the viscoelastic effects on moving contact lines in the context of phase-field modeling. Unlike slip models, the phase-field model reveals detailed flow patterns in the inner region of the contact line, which feature strong shearing below a stagnation point. This enables us to capture qualitatively the viscoelastic effects observed in the experiments. First, the polymer stress generated in the inner region tends to enhance bending if polymers are on the advancing side of the interface, and reduce bending if the polymers are on the receding side. However, due to the small size of the inner region, the effect on the macroscopic flow is small. Second, due to the limited residence time in the inner region, the strong shear flow only highlights the relaxation modes with effective Weissenberg number close to one. As a result, the observed viscoelastic effects actually come from the weakly elastic oligomeric solvent of the Boger fluids rather than the HMW polymers. Finally, we emphasize the phenomenological nature of the phase-field model. The microscopic physics in the inner region of the contact line is unknown, and maybe unknowable. The model prediction is not intended as a true picture of that. Rather, it is used to construct a plausible explanation of the experimentally observed viscoelastic effects on moving contact lines.

Acknowledgments. The authors thank S. Garoff, E. Ramé and L. M. Walker for helpful discussions. P.Y. acknowledges the support by NSF-DMS 0907788. J.J.F. acknowledges support by the Petroleum Research Fund, the Canada Research Chair program, NSERC (Discovery and Strategic grants and Accelerator Supplement) and the Canada Foundation for Innovation.

References

[1] C. Huh, L. E. Scriven, Hydrodynamic model of steady movement of a solid/liquid/fluid contact line, J. Colloid Interface Sci. 35 (1971) 85–101.

[2] E. B. Dussan V., On the spreading of liquids on solid surfaces: static and dynamic contact lines, Annu. Rev. Fluid Mech. 11 (1979) 371–400.

[3] M. A. Spaid, G. M. Homsy, Stability of Newtonian and viscoelastic dynamic contact lines, Phys. Fluids 8 (1996) 460–478.

[4] E. B. Dussan V., The moving contact line: the slip boundary condition, J. Fluid Mech. 77 (1976) 665–684.

[5] D. Jacqmin, Contact-line dynamics of a diffuse fluid interface, J. Fluid Mech. 402 (2000) 57–88.

[6] Y. Wei, E. Ramé, L. M. Walker, S. Garoff, Dynamic wetting with viscous Newtonian and non-Newtonian fluids, J. Phys.: Condens. Matter 21 (2009) 464126.

[7] P. Yue, C. Zhou, J. J. Feng, Sharp-interface limit of the Cahn-Hilliard model for moving contact lines, J. Fluid Mech. 645 (2010) 279–294.

[8] Q. Min, Y.-Y. Duan, X.-D. Wang, Z.-P. Liang, C. Si, Does macroscopic flow geometry influence wetting dynamic?, J. Colloid Interface Sci. 362 (2011) 221–227.

[9] E. Ramé, S. Garoff, K. R. Willson, Characterizing the microscopic physics near moving contact lines using dynamic contact angle data, Phys. Rev. E 70 (2004) 031608.

[10] A. V. Borkar, J. A. Tsamopoulos, S. A. Gupta, R. K. Gupta, Spin coating of viscoelastic and nonvolatile fluids over a planar disk, Phys. Fluids 6 (2007) 3539–3553.

[11] M. Bajaj, J. R. Prakash, M. Pasquali, A computational study of the effect of viscoelasticity on slot coating flow of dilute polymer solutions, J. Non-Newtonian Fluid Mech. 149 (2008) 104–123.

[12] A. Abedijaberi, G. Bhatara, E. S. G. Shaqfeh, B. Khomami, A computational study of the influence of viscoelasticity on the interfacial dynamics of dip coating flow, J. Non-Newtonian Fluid Mech. 166 (2011) 614–627.

[13] N. Fraysse, G. M. Homsy, An experimental study of rivulet instabilities in centrifugal spin coating of viscous Newtonian and non-Newtonian fluids, Phys. Fluids 6 (1994) 1491–1504.

[14] G. K. Seevaratnam, L. M. Walker, E. Ramé, S. Garoff, Wetting by simple room-temperature polymer melts: deviations from Newtonian behavior, J. Colloid Interface Sci. 284 (2005) 265–270.

[15] G. K. Seevaratnam, Y. Suo, E. Ramé, L. M. Walker, S. Garoff, Dynamic wetting of shear thinning fluids, Phys. Fluids 19 (2007) 012103.

[16] Y. Wei, G. K. Seevaratnam, S. Garoff, E. Ramé, L. M. Walker, Dynamic wetting of boger fluids, J. Colloid Interface Sci. 313 (2007) 274–820.

[17] Y. Wei, S. Garoff, L. M. Walker, Impact of fluid memory on wetting approaching the air entrainment limit, J. Colloid Interface Sci. 337 (2009) 619–621.

[18] E. B. Dussan V., E. Rame, S. Garoff, On identifying the appropriate boundary conditions at a moving contact line: an experimental investigation, J. Fluid Mech. 230 (1991) 97–116.

[19] Y. Wei, Dynamic wetting of viscous and viscoelastic fluids, Ph.D. thesis, Carnegie Mellon University (2009).

[20] M. A. Spaid, G. M. Homsy, Viscoelastic free surface flows: spin coating and dynamic contact lines, J. Non-Newtonian Fluid Mech. 55 (1994) 249–281.

[21] P. Yue, J. J. Feng, C. Liu, J. Shen, A diffuse-interface method for simulating two-phase flows of complex fluids, J. Fluid Mech. 515 (2004) 293–317.

[22] R. B. Bird, A. R. C., O. Hassager, Dynamics of Polymeric Liquids, Vol. 1. Fluid Mechanics, Wiley, New York, 1987.

[23] P. Yue, J. J. Feng, Wall energy relaxation in the Cahn-Hilliard model for moving contact lines, Phys. Fluids 23 (2011) 012106.

[24] P. Yue, J. J. Feng, Can diffuse-interface models quantitatively describe moving contact lines?, Eur. Phys. J. - Spec. Top. 197 (2011) 37–46.

[25] P. Yue, C. Zhou, J. J. Feng, C. F. Ollivier-Gooch, H. H. Hu, Phase-field simulations of interfacial dynamics in viscoelastic fluids using finite elements with adaptive meshing, J. Comput. Phys. 219 (2006) 47–67.

[26] X. Chen, E. Ramé, S. Garoff, The effects of thin and ultrathin films on dynamic wetting, Phys. Fluids 16 (2004) 287–297.

[27] R. G. Cox, The dynamics of the spreading of liquids on a solid surface. Part 1. Viscous flow, J. Fluid Mech. 168 (1986) 168–194.

[28] G. K. Seevaratnam, Dynamic wetting of non-Newtontian fluids, Ph.D. thesis, Carnegie Mellon University (2006).

[29] P. C. Wayner, J. Schonberg, Spreading of a liquid film on a substrate by the evaporation-adsorption process, J. Colloid Interface Sci. 152 (1992) 507–520.

[30] P. Seppecher, Moving contact lines in the Cahn-Hilliard theory, Int. J. Eng. Sci. 34 (1996) 977–992.

[31] J. H. Kim, W.-X. Shi, R. G. Larson, Methods of stretching DNA molecules using flow fields, Langmuir 23 (2007) 755–764.

[32] M. I. Smith, V. Bertola, Effect of polymer additives on the wetting of impacting droplets, Phys. Rev. Lett. 104 (2010) 154502.